Published in final edited form as:
Nature. ; 482(7384): 232–236. doi:10.1038/nature10771.

High-throughput decoding of anti-trypanosomal drug efficacy and resistance

Sam Alsford[1], **Sabine Eckert**[2,4], **Nicola Baker**[1], **Lucy Glover**[1], **Alejandro Sanchez-Flores**[2], **Ka Fai Leung**[3], **Daniel J. Turner**[2,4], **Mark C. Field**[3], **Matthew Berriman**[2], and **David Horn**[1,§]

[1]London School of Hygiene & Tropical Medicine, Keppel Street, London, WC1E 7HT, UK.

[2]The Wellcome Trust Sanger Institute, Hinxton, Cambridge, CB10 1SA, UK.

[3]Department of Pathology, University of Cambridge, Tennis Court Road, Cambridge, CB2 1QP, UK

Summary

The concept of specific chemotherapy was developed a century ago by Paul Ehrlich and others. Dyes and arsenical compounds that displayed selectivity against trypanosomes were central to this work [1,2], and the drugs that emerged remain in use for treating Human African Trypanosomiasis (HAT) [3]. Ehrlich recognised the importance of understanding the mechanisms underlying selective drug action and resistance for the development of improved HAT therapies, but these mechanisms have remained largely mysterious. Here, we use all five current HAT drugs for genome-scale RNA interference (RNAi) target sequencing (RIT-seq) screens in *Trypanosoma brucei*, revealing the transporters, organelles, enzymes and metabolic pathways that function to facilitate anti-trypanosomal drug action. RIT-seq profiling identifies both known drug importers [4,5] and the only known pro-drug activator [6], and links more than fifty additional genes to drug action. A specific bloodstream stage invariant surface glycoprotein (ISG75) family mediates suramin uptake while the AP-1 adaptin complex, lysosomal proteases and major lysosomal *trans*membrane protein, as well as spermidine and *N*-acetylglucosamine biosynthesis all contribute to suramin action. Further screens link ubiquinone availability to nitro-drug action, plasma membrane P-type H^+-ATPases to pentamidine action, and trypanothione and multiple putative kinases to melarsoprol action. We also demonstrate a major role for aquaglyceroporins in pentamidine and melarsoprol cross-resistance. These advances in our understanding of mechanisms of anti-trypanosomal drug efficacy and resistance will aid the rational design of new therapies and help to combat drug resistance, and provide unprecedented levels of molecular insight into the mode of action of anti-trypanosomal drugs.

Keywords

DFMO; eflornithine; ISG75; nifurtimox; RNAi

[§]To whom correspondence should be addressed. david.horn@lshtm.ac.uk .
[4]Current address: Oxford Nanopore Technologies, 4 Robert Robinson Avenue, Oxford, OX4 4GA, UK

Author Contributions S.A., N.B., L.G. and K.F.L. carried out the *T. brucei* manipulation and analyses; S.E., A.S. and D.J.T. carried out the Illumina sequencing and mapping; D.H. coordinated the study and S.A., M.C.F., M.B. and D.H. wrote the paper.

Full Methods and any associated references are available in the online version of the paper at www.nature.com/nature.

Supplementary Information is linked to the online version of the paper at www.nature.com/nature.

Author Information Sequence data from this study have been submitted to the European Nucleotide Archive at http://www.ebi.ac.uk/ena under accession no. ERA071064.

The authors have no competing financial interests to declare.

African trypanosomes are transmitted by the tsetse insect vector and circulate in the bloodstream and tissue fluids of their mammalian hosts. These protozoan parasites cause Human African Trypanosomiasis (HAT), also known as sleeping sickness, and the livestock disease known as Nagana. HAT is typically fatal without chemotherapeutic intervention. The public health situation has improved recently with increased monitoring and chemotherapy averting more than 1.3 million DALYs (Disability-Adjusted Life Years) during 2000 and cases estimated at less than 70,000 in 2006 [7]. However, therapies suffer multiple problems including severe toxicity and increasing resistance, a major concern due to the absence of a vaccine or therapeutic alternatives [3]. The current HAT therapies are pentamidine or suramin, which are only suitable for the first stage of the disease prior to central nervous system involvement, and eflornithine, nifurtimox or melarsoprol for advanced disease [3] (Supplementary Table 1). Developed well before the advent of molecular, target-based therapy, all of these drugs, except for eflornithine, elicit their anti-trypanosomal effects by disrupting unknown targets. Increasing HAT treatment failure rates were reported for suramin, when this drug was still in use in West Africa in the 1950s [8], while melarsoprol treatment failure is a current and increasing problem [9].

We used genome-scale tetracycline-inducible RNA interference (RNAi) library screens in *Trypanosoma brucei* to identify the genes that contribute to drug action. In these screens, knockdowns only persist in an otherwise toxic environment if they confer a selective advantage while others are diminished or eliminated (Fig. 1a); note that knockdown is not expected to identify drug targets. The RNAi library consists of ~750,000 clones, each transformed with one RNAi construct, and representing >99% of the approximately 7,500 non-redundant *T. brucei* gene set. Because each gene is identified by an average of approximately five different RNAi sequences, true leads can be identified with high confidence and potential off-target false leads can be minimised (see Supplementary Methods). Screens were performed using all current HAT drugs and each yielded a population of cells displaying an inducible drug resistance phenotype after eight or fourteen days of selection (Fig. 1b and Supplementary Fig. 1). Genomic DNA from these cells was subjected to RNAi target sequencing (RIT-seq) [10] to create profiles of RNAi targets associated with increased resistance, and to identify the genes that contribute to drug susceptibility. Genome-wide association maps show read-density for 7,435 *T. brucei* genes (Fig. 1c). We defined genes with ‘primary signatures’ as those associated with two or more independent RIT-seq tags, each with a read-density of >99; the screens yielded 55 of these signatures (red bars in Fig. 1c; see Supplementary Methods and Supplementary data File 1). Previous work linked the P2 adenosine transporter (AT1) to melarsoprol uptake [4,11-13], an amino acid transporter (AAT6) to eflornithine uptake [5,13,14] and a nitroreductase (NTR) to nifurtimox activation [6,14]. Each of these genes is identified on the appropriate genome-wide association map (Fig. 1c), providing validation for our screens and indicating excellent genome-scale coverage in the RNAi library. Selected read-density signatures that establish new genetic links to drug susceptibility are shown in Figure 1d.

The known eflornithine transporter is the only primary signature from the eflornithine screen. In striking contrast, the suramin screen revealed twenty-eight genes associated with primary signatures (Fig. 1c and Supplementary data File 1). Suramin, used for HAT therapy since the 1920s [15], is a colourless sulphated napthylamine related to Ehrlich’s trypan red. This drug cannot cross lipid membranes by passive diffusion due to strong negative charge. Genes linked to suramin action encode a bloodstream stage-specific invariant surface glycoprotein (ISG75) of unknown function [16], four lysosomal proteins (the CatL and CBP1 peptidases, p67 and Golgi/lysosomal protein-1, GLP-1), all four subunits of the adaptin complex (AP) 1, involved in endosomal, clathrin-mediated trafficking, and multiple

spermidine and *N*-acetylglucosamine (NAG) biosynthetic enzymes (Supplementary Fig. 2 and Supplementary data File 1).

Eight of these genes were selected for further analysis. We assembled multiple independent inducible RNAi strains for each gene and confirmed that knockdown (Fig. 2a, Supplementary Fig. 3) increased suramin resistance in every case (Fig. 2b, Supplementary Fig. 4). We then determined subcellular localisation for the putative major facilitator superfamily transporter (MFST); the *MFST* gene gave the strongest read-density signature in the suramin screen and the greatest effective 50% inhibitory concentration (EC_{50}) increase (>10-fold) following knockdown (Fig. 2b). MFST, and a member of the endo-membrane protein 70 family (EMP70), in contrast to UbH1, partitioned into the *T. brucei* membrane fraction, as expected (Fig. 2c), and MFST localised to the lysosome, along with the major lysosomal type I membrane glycoprotein, p67 [17], also identified in the screen (Fig. 2d). Because ISG75 trafficking is ubiquitin-dependent [18] we investigated whether UbH1, a putative ubiquitin hydrolase identified by the screen, influenced ISG75 expression. UbH1 knockdown reduced ISG75 but not ISG65 expression (Fig. 2e), suggesting that deubiquitination by UbH1 specifically affects ISG75 copy number; clearly this mimics the direct effect of RNAi against ISG75. A vacuolar protein sorting factor, Vps5, that positively controls ISG75 expression [19], and a second putative ubiquitin hydrolase, were also identified by the screen (see Supplementary Fig. 2 and Supplementary data File 1), suggesting that ISG75 copy number is highly connected to suramin resistance. To ask if ISG75 contributes to suramin binding, we performed whole-cell binding-assays using ^{3}[H]-labelled suramin. Cells depleted for ISG75 displayed significantly and specifically reduced suramin binding (Fig. 2f).

We observed >4-fold increase in EC_{50} following knockdown of the cathepsin-L (CatL) like protease known as brucipain, another abundant lysosomal protein [20], and an orthogonal assay using a dual-specificity CatL/CatB inhibitor revealed inhibitor antagonism (Fig. 2g), indicating that protease activity enhances suramin toxicity. Taken together, the results demonstrate a central role for lysosomal functions in suramin action. Since four enzymes involved in spermidine biosynthesis, including ornithine decarboxylase (ODC), were linked to suramin action (Supplementary data File 1), we used eflornithine to specifically inhibit ODC, which again revealed inhibitor antagonism (Fig. 2g; see note b in Supplementary Table 1). Thus, ODC activity enhances suramin toxicity, likely through spermidine biosynthesis. Suramin endocytosis [21] and intralysosomal accumulation [22] have been demonstrated previously in *T. brucei*. In addition, an acquired suramin resistance phenotype was stable in bloodstream stage *T. brucei* but was not expressed in the insect stage [23]. Our RIT-seq profile, stage-specific expression of ISG75 [16] and strong down-regulation of endocytic and lysosomal activities in the insect stage [24], are all consistent with these observations.

Paul Ehrlich's work with dyes and arsenicals revealed the first examples of resistance to chemotherapy a century ago and, based on cross-resistance, he deduced that there are shared mechanisms contributing to the action of certain 'parasitotropic' compounds [1]. Among current HAT therapies, cross-resistance has been documented only for melarsoprol and pentamidine [9] but our understanding of the mechanism remains incomplete. Both drugs enter trypanosomes through the P2 adenosine transporter, but additional, dual-specificity transporters are predicted [9]. To identify cross-resistance mechanisms, we analysed all pair-wise comparisons among our screens (Fig. 3a). A single robust signature emerged, implicating two closely related aquaglyceroporins (AQPs) [25] in melarsoprol and pentamidine cross-resistance. To directly test the role of the AQPs, we generated *aqp2/3* null strains (Fig. 3b). The EC_{50} for melarsoprol and pentamidine was increased >2-fold and >15-

fold, respectively, in *aqp2/3* null cells compared to wild-type (Fig. 3c). Our favoured hypothesis involves regulation of dual-specificity transporters by AQPs.

The nifurtimox, pentamidine and melarsoprol screens yielded eight, nine and nine genes associated with primary signatures, respectively. The major primary signature in the nifurtimox profile identified the mitochondrial, flavin-dependent nitroreductase that activates this class of nitro pro-drugs [6]. We also identified the putative flavokinase which converts riboflavin to FMN, an essential nitroreductase cofactor [6]. Four additional signatures identified genes encoding proteins linked to ubiquinone biosynthesis (Supplementary Fig. 2 and Supplementary data File 1), in support of the hypothesis that nitroreductase, like NADH dehydrogenases, transfers electrons from NADH to ubiquinone (UQ-9) to generate ubiquinol [6]. We assembled RNAi strains for one of these factors and demonstrated that knockdown increased the EC_{50} for nifurtimox by approximately 1.5-fold (Supplementary Fig. 5). Thus, six gene signatures support a dominant role for nitroreductase in nifurtimox activation and suggest that this is dependent upon the availability of the FMN cofactor and the natural substrate.

Pentamidine is an aromatic diamidine, a nucleic acid binding drug that accumulates to millimolar concentrations and collapses trypanosome mitochondrial membrane potential [26]. Two primary signatures from the pentamidine screen identify genes encoding P-type ATPases (Supplementary Fig. 2 and Supplementary data File 1), and one of these represents the plasma membrane H^+-ATPases, HA1-3 [27]. We assembled RNAi strains for these ATPases and demonstrated that knockdown increased the EC_{50} for pentamidine by >8-fold (Supplementary Fig. 5), suggesting that an HA1-3 dependent proton motive force is required to drive pentamidine uptake. We used a similar approach to demonstrate >2-fold increase in the EC_{50} for pentamidine following knockdown of a putative protein phosphatase (Supplementary Fig. 5).

Melarsoprol acts primarily by forming a stable adduct with trypanothione, known as Mel T [28], but whether this adduct reduces or increases toxicity has remained unclear. The melarsoprol screen identified a link to trypanothione synthase and trypanothione reductase (Supplementary Fig. 2 and Supplementary data File. 1), suggesting that the Mel T adduct is toxic. Three other primary signatures identified an over-representation ($P=2.3\times10^{-9}$, χ^2 test) of putative protein kinases (Supplementary Fig. 2 and Supplementary data File. 1) while another signature identified a gene encoding a highly phosphorylated protein related to the *N*-terminal segment of the LArge Tumor Suppressor, LATS1 (see Supplementary Fig. 2a). We used independent strains to confirm that LATS1-like knockdown increased the EC_{50} for melarsoprol by approximately 1.5-fold (Supplementary Fig. 5). Based on these signatures, we suggest a role for a signalling cascade in melarsoprol susceptibility. Our findings are summarised in Figure 4. In particular, we propose suramin uptake via ISG75-mediated endocytosis (Fig. 4a). Metabolic pathways that contribute to suramin or nifurtimox action are detailed in Figure 4b.

All but one of the current HAT drugs was developed in the absence of an understanding of the chemical-biological relationships underlying toxicity or selectivity. Our RIT-seq profiles revealed more than fifty *T. brucei* genes that enhance drug susceptibility, unearthing interactions that are largely inaccessible using other approaches. Notably, the knockdown approach and the sensitivity of RIT-seq allow access to essential proteins, complexes and pathways, such as the H^+-ATPase, the adaptin complex and spermidine biosynthesis. Our results also illustrate the utility of drugs as molecular probes for functional networks. In particular, the findings highlight factors that contribute to drug accumulation or the generation of toxic metabolites, features that could be exploited to deliver or generate novel toxins. Additionally, absence or loss of function could explain innate or acquired resistance;

suramin or melarsoprol/pentamidine resistance may be due to reduced MFST or AQP expression, respectively, for example (Supplementary Fig. 6). These advances in our understanding of drug-trypanosome interactions will facilitate rational approaches to the design of more efficacious and durable therapies, and for monitoring the emergence and spread of resistance.

METHODS SUMMARY

Assembly of the bloodstream-form *T. brucei* RNAi library and RNAi target sequencing (RIT-seq) were reported previously [10]. Briefly, a tetracycline-inducible RNAi plasmid library, containing randomly sheared genomic fragments (mean ~600 bp) under the control of head-to-head, tetracycline-inducible phage T7 promoters [29], was targeted to a single genomic locus that had been validated for robust expression [30]. The long double-stranded RNAs generated in the presence of tetracycline are processed to produce a pool of small-interfering RNAs that programme the endogenous RNAi machinery to mediate sequence-specific destruction of the cognate mRNA. For this study, the library was grown under inducing conditions with drug selection and genomic DNA was isolated from surviving populations. For RIT-seq profiling, adapter-ligated sequencing libraries were prepared from each genomic DNA sample and used to amplify DNA fragments containing RNAi cassette-insert junctions in semi-specific PCR reactions; one primer was specific for the RNAi vector and the other for the Illumina adapter. Size-selected DNA was sequenced with 76 cycle runs on an Illumina GAII. Sequencing reads containing a nine-base RNAi cassette-insert junction sequence were then mapped to the *T. brucei* reference genome. Where loss of function increases drug tolerance, RNAi-target sequence representation is increased relative to the otherwise susceptible population, revealing ‘hot spots’. Thus, RNAi target fragments serve as templates for the production of dsRNA and also provide unique sequence identifiers for each clonal population.

METHODS

T. brucei growth and drug selection

The bloodstream-form *T. brucei* MiTat 1.2, clone 221a RNAi library [10] was derived using the randomly sheared genomic fragment (mean ~600 bp) RNAi plasmid library [29]. The *T. brucei* RNAi library and 2T1 cells [30] were maintained as described. For selective screens, the RNAi library, maintained throughout at $>5\times10^6$ cells, was induced with tetracycline (Tet; 1 μg ml^{-1}) for 24 h and then grown in medium containing Tet, plus each HAT drug at 0.5 to 3.5 × EC_{50} (Supplementary Table 1; Supplementary Fig. 1); all drug stocks were in DMSO.

RNAi target sequencing (RIT-seq)

Selected populations from each screen were assessed for Tet-dependent drug-resistance. The RNAi target fragments provide unique identifiers for each clone in the population. As a quality-control step, PCR amplification, agarose gel fractionation and Sanger sequencing of the eluted products were performed as described [14], followed by RIT-seq analysis [10]; all nine genes identified by Sanger sequencing were associated with high-density Illumina read-counts (13,000 to 528,000; see Supplementary data File 1a). Briefly, we ran 76 cycle sequencing on an Illumina GAII; this generates sequence tags derived from the ends of the RNAi target fragments. Only sequences containing a terminal RNAi-vector junction sequence (GCCTCGCGA) were mapped to the *T. brucei* 927 reference genome [31] using the SSAHA sequence alignment algorithm [32]. After mapping, we obtained, for each protein coding sequence (CDS) in each experiment, a count of reads mapping; all genes associated with >9 reads are detailed in Supplementary data File 1b. We also browsed all read-density

plots in Artemis [33] for signatures that fell outside of CDSs to generate the full non-redundant 'hit-list' detailed in Supplementary data File 1a.

Read-density signatures

Genome coverage in the current RNAi library represents >99% of all genes, with 5 RNAi targets per gene on average [10]; shorter genes are expected to be represented by fewer RNAi targets. Our screens yielded 5 to 59 genes (0.07 – 0.8 %) with a $^{>99}$RIT-seq tag (a tag with a read density of >99; eflornithine, 5; suramin, 59; nifurtimox, 54; pentamidine, 17 and melarsoprol, 19). In each screen, at least one gene was associated with a $^{>50,000}$RIT-seq tag (Supplementary data File 1a). From this set, we derived 55 genes with 'primary signatures', those associated with two or more $^{>99}$RIT-seq tags. If these tags were randomly distributed, we would expect a single primary signature from 300 screens using eflornithine or from two screens using suramin, assigning a high degree of confidence to the vast majority of observed primary signatures (Supplementary data File 1a). The nifurtimox output is unusual compared to the other outputs and may reflect drug-mediated mutagenesis [34]; inactivating mutations within *NTR*, for example, may prolong the survival of clones carrying unrelated RNAi targets. However, even limited Tet-regulated drug resistance (Fig. 1b) and a high number of sequence tags in the nifurtimox screening profile (Supplementary data File 1 and black bars in Fig. 1c) had little impact on primary signature confidence. Many of the 130 genes associated with 'secondary signatures' in Supplementary data File 1a may also reflect mechanisms of drug action, but we only considered seven of these genes here that were linked to a common function with a primary hit (Supplementary Fig. 2). We observe 3.5 tags per gene on average associated with the 24 primary, single copy genes shown in Supplementary Figure 2. Minimal library propagation could explain a modest reduction in coverage but we suggest that reduced coverage in the current RIT-seq outputs is primarily explained by major fitness defects following knockdown.

Plasmid construction and strain assembly

The *AQP* locus was disrupted by replacement of a 4,772 bp (*aqp2*/*aqp3*) fragment with *NPT* and *BLA* selectable markers (the *T. brucei* genome is diploid). Gene-specific RNAi fragments of 400-600 bp, or 200 bp to facilitate moderate knockdown in the case of the known essential gene p67 [17], were amplified using PCR primers designed using RNAit [35] and cloned into pRPa^{iSL} for the generation of stem-loop, 'hairpin' dsRNA as the trigger for RNAi [36]. We used a long, 400-600 bp RNAi target fragment for CatL because RNAi previously produced no growth defect [37]. However, cells retained 35% CatL activity in that study, likely explaining why we see a major growth defect when expressing a more potent stem-loop dsRNA (Supplementary Fig. 3). For epitope tagging at native loci, *C*-terminal fragments, or an *N*-terminal fragment (UbH1), were amplified and cloned in pNATx^{TAG} or pNAT^{TAG}x [36], respectively. Constructs were introduced into 2T1 cells as described [30]. Full oligonucleotide details are available on request.

Strain analysis

Cumulative growth curves were generated from cultures seeded at 10^5 cells ml^{-1}, counted on a haemocytometer and diluted back to 10^5 cells ml^{-1} as necessary. For EC_{50} assays, RNAi strains were pre-induced for 72 h in 1 μg ml^{-1} tetracycline, except CatL and AP-1β, which were pre-induced for 24 h at 2.5 and 1 ng ml^{-1}, respectively. Isobolograms were generated using a checkerboard assay as described [38]; FMK024 (N-Morpholineurea-phenylalanyl-homophenylalanylfluoromethyl ketone, Sigma) is an irreversible, dual-specificity inhibitor of CatL/CatB. All EC_{50} assays were carried out using alamarBlue as described [14,39]. Southern blotting was carried out according to standard procedures [40]. Sub-cellular fractionation by hypotonic lysis was carried out as described [41]. All protein samples were stored in the presence of a protease inhibitor cocktail (Roche) and were not boiled.

Whole cell lysates and hypotonic lysis fractions were separated by SDS-PAGE using standard protocols [40]. Immunofluorescence was carried out as previously described [10]. We used specific antisera to detect ISG75 [42], p67 [43], CatL [17], GLP-1 [44] and AP-1γ [45] while anti MYC antisera were used to detect tagged versions of MFST, UbH1 and EMP70. To assess suramin binding, cells were harvested at mid-log phase and resuspended at 10^7 ml^{-1} in 35 nM ^{3}[H]-suramin (Hartmann Analytic; pre-incubated for 16 hours in complete HMI11) at 37°C. Cells were washed in ice cold PBS, resuspended in 100 μl Optiphase Supermix scintillant (Perkin Elmer) and ^{3}[H]-suramin incorporation quantified using a 1450 Microbeta scintillation counter (Perkin Elmer).

References

31. Berriman M, et al. The genome of the African trypanosome *Trypanosoma brucei*. Science. 2005; 309:416–422. [PubMed: 16020726]
32. Ning Z, Cox AJ, Mullikin JC. SSAHA: a fast search method for large DNA databases. Genome Res. 2001; 11:1725–1729. [PubMed: 11591649]
33. Carver T, et al. Artemis and ACT: viewing, annotating and comparing sequences stored in a relational database. Bioinformatics. 2008; 24:2672–2676. [PubMed: 18845581]
34. Buschini A, et al. Genotoxicity revaluation of three commercial nitroheterocyclic drugs: nifurtimox, benznidazole, and metronidazole. J Parasitol Res. 2009; 2009:463575. [PubMed: 20981287]
35. Redmond S, Vadivelu J, Field MC. RNAit: an automated web-based tool for the selection of RNAi targets in *Trypanosoma brucei*. Mol Biochem Parasitol. 2003; 128:115–118. [PubMed: 12706807]
36. Alsford S, Horn D. Single-locus targeting constructs for reliable regulated RNAi and transgene expression in *Trypanosoma brucei*. Mol Biochem Parasitol. 2008; 161:76–79. [PubMed: 18588918]
37. Mackey ZB, O'Brien TC, Greenbaum DC, Blank RB, McKerrow JH. A cathepsin B-like protease is required for host protein degradation in *Trypanosoma brucei*. J Biol Chem. 2004; 279:48426–48433. [PubMed: 15326171]
38. Singh PK, Tack BF, McCray PB Jr. Welsh MJ. Synergistic and additive killing by antimicrobial factors found in human airway surface liquid. Am J Physiol Lung Cell Mol Physiol. 2000; 279:L799–805. [PubMed: 11053013]
39. Raz B, Iten M, Grether-Buhler Y, Kaminsky R, Brun R. The Alamar Blue assay to determine drug sensitivity of African trypanosomes (*T.b. rhodesiense* and *T.b. gambiense*) *in vitro*. Acta Trop. 1997; 68:139–147. [PubMed: 9386789]
40. Ausubel, FM., et al. Curr. Proto. Mol. Biol. John Wiley and Sons, Inc.; 1998.
41. Leung KF, Dacks JB, Field MC. Evolution of the multivesicular body ESCRT machinery; retention across the eukaryotic lineage. Traffic. 2008; 9:1698–1716. [PubMed: 18637903]
42. Ziegelbauer K, Overath P. Organization of two invariant surface glycoproteins in the surface coat of *Trypanosoma brucei*. Infect Immun. 1993; 61:4540–4545. [PubMed: 8406850]
43. Kelley RJ, Brickman MJ, Balber AE. Processing and transport of a lysosomal membrane glycoprotein is developmentally regulated in African trypanosomes. Mol Biochem Parasitol. 1995; 74:167–178. [PubMed: 8719158]
44. Lingnau A, Zufferey R, Lingnau M, Russell DG. Characterization of tGLP-1, a Golgi and lysosome-associated, transmembrane glycoprotein of African trypanosomes. J Cell Sci. 1999; 112(Pt 18):3061–3070. [PubMed: 10462522]
45. Allen CL, Liao D, Chung WL, Field MC. Dileucine signal-dependent and AP-1-independent targeting of a lysosomal glycoprotein in *Trypanosoma brucei*. Mol Biochem Parasitol. 2007; 156:175–190. [PubMed: 17869353]

Supplementary Material

Refer to Web version on PubMed Central for supplementary material.

Acknowledgments

We thank James Morris, Zefeng Wang, Mark Drew and Paul Englund for the RNAi plasmid library, Vanessa Yardley for anti-trypanosomal drugs, James Bangs for anti p67 and CatL sera, David Russell for anti GLP-1 sera and John Kelly, Martin Taylor and Brendan Wren for comments on the draft manuscript. The work was funded by grants from The Wellcome Trust (093010/Z/10/Z at the LSHTM, 085775/Z/08/Z at The Wellcome Trust Sanger Institute and 090007/Z/09/Z at The University of Cambridge). N.B. was supported by a Bloomsbury colleges PhD studentship.

References

1. Ehrlich P. Address in Pathology, on chemiotherapy: Delivered before the Seventeenth International Congress of Medicine. Br Med J. 1913; 2:353–359. [PubMed: 20766753]
2. Williamson, J.; Mulligan, HW. Review of chemotherapeutic and chemoprophylactic agents. The African Trypanosomiaises. 1970.
3. Fairlamb AH. Chemotherapy of human African trypanosomiasis: current and future prospects. Trends Parasitol. 2003; 19:488–494. [PubMed: 14580959]
4. Maser P, Sutterlin C, Kralli A, Kaminsky R. A nucleoside transporter from *Trypanosoma brucei* involved in drug resistance. Science. 1999; 285:242–244. [PubMed: 10398598]
5. Vincent IM, et al. A molecular mechanism for eflornithine resistance in African trypanosomes. PLoS Pathog. 2010; 6:e1001204. [PubMed: 21124824]
6. Wilkinson SR, Taylor MC, Horn D, Kelly JM, Cheeseman I. A mechanism for cross-resistance to nifurtimox and benznidazole in trypanosomes. Proc Natl Acad Sci U S A. 2008; 105:5022–5027. [PubMed: 18367671]
7. Fevre EM, Wissmann BV, Welburn SC, Lutumba P. The burden of human African trypanosomiasis. PLoS Negl Trop Dis. 2008; 2:e333. [PubMed: 19104653]
8. Pepin J, Milord F. The treatment of human African trypanosomiasis. Adv Parasitol. 1994; 33:1–47. [PubMed: 8122565]
9. de Koning HP. Ever-increasing complexities of diamidine and arsenical crossresistance in African trypanosomes. Trends Parasitol. 2008; 24:345–349. [PubMed: 18599351]
10. Alsford S, et al. High-throughput phenotyping using parallel sequencing of RNA interference targets in the African trypanosome. Genome Res. 2011; 21:915–924. [PubMed: 21363968]
11. Carter NS, Fairlamb AH. Arsenical-resistant trypanosomes lack an unusual adenosine transporter. Nature. 1993; 361:173–176. [PubMed: 8421523]
12. Matovu E, et al. Mechanisms of arsenical and diamidine uptake and resistance in *Trypanosoma brucei*. Eukaryot Cell. 2003; 2:1003–1008. [PubMed: 14555482]
13. Schumann Burkard G, Jutzi P, Roditi I. Genome-wide RNAi screens in bloodstream form trypanosomes identify drug transporters. Mol Biochem Parasitol. 2011; 175:91–94. [PubMed: 20851719]
14. Baker N, Alsford S, Horn D. Genome-wide RNAi screens in African trypanosomes identify the nifurtimox activator NTR and the eflornithine transporter AAT6. Mol Biochem Parasitol. 2011; 176:55–57. [PubMed: 21093499]
15. Steverding D. The development of drugs for treatment of sleeping sickness: a historical review. Parasit Vectors. 2010; 3:15. [PubMed: 20219092]
16. Overath P, Chaudhri M, Steverding D, Ziegelbauer K. Invariant surface proteins in bloodstream forms of *Trypanosoma brucei*. Parasitol Today. 1994; 10:53–58. [PubMed: 15275499]
17. Peck RF, et al. The LAMP-like protein p67 plays an essential role in the lysosome of African trypanosomes. Mol Microbiol. 2008; 68:933–946. [PubMed: 18430083]
18. Leung KF, Riley FS, Carrington M, Field MC. Ubiquitylation and developmental regulation of invariant surface protein expression in trypanosomes. Eukaryot Cell. 2011; 10:916–931. [PubMed: 21571921]
19. Koumandou VL, et al. Evolutionary reconstruction of the retromer complex and its function in *Trypanosoma brucei*. J Cell Sci. 2011; 124:1496–1509. [PubMed: 21502137]

20. Caffrey CR, et al. Active site mapping, biochemical properties and subcellular localization of rhodesain, the major cysteine protease of *Trypanosoma brucei rhodesiense*. Mol Biochem Parasitol. 2001; 118:61–73. [PubMed: 11704274]

21. Fairlamb AH, Bowman IB. Uptake of the trypanocidal drug suramin by bloodstream forms of *Trypanosoma brucei* and its effect on respiration and growth rate *in vivo*. Mol Biochem Parasitol. 1980; 1:315–333. [PubMed: 6108510]

22. Vansterkenburg EL, et al. The uptake of the trypanocidal drug suramin in combination with low-density lipoproteins by *Trypanosoma brucei* and its possible mode of action. Acta Trop. 1993; 54:237–250. [PubMed: 7902661]

23. Scott AG, Tait A, Turner CM. Characterisation of cloned lines of *Trypanosoma brucei* expressing stable resistance to MelCy and suramin. Acta Trop. 1996; 60:251–262. [PubMed: 8659324]

24. Natesan SK, Peacock L, Matthews K, Gibson W, Field MC. Activation of endocytosis as an adaptation to the mammalian host by trypanosomes. Eukaryot Cell. 2007; 6:2029–2037. [PubMed: 17905918]

25. Uzcategui NL, et al. Cloning, heterologous expression, and characterization of three aquaglyceroporins from *Trypanosoma brucei*. J Biol Chem. 2004; 279:42669–42676. [PubMed: 15294911]

26. Lanteri CA, Tidwell RR, Meshnick SR. The mitochondrion is a site of trypanocidal action of the aromatic diamidine DB75 in bloodstream forms of *Trypanosoma brucei*. Antimicrob Agents Chemother. 2008; 52:875–882. [PubMed: 18086841]

27. Luo S, Fang J, Docampo R. Molecular characterization of *Trypanosoma brucei* P-type H^+-ATPases. J Biol Chem. 2006; 281:21963–21973. [PubMed: 16757482]

28. Fairlamb AH, Henderson GB, Cerami A. Trypanothione is the primary target for arsenical drugs against African trypanosomes. Proc Natl Acad Sci U S A. 1989; 86:2607–2611. [PubMed: 2704738]

29. Morris JC, Wang Z, Drew ME, Englund PT. Glycolysis modulates trypanosome glycoprotein expression as revealed by an RNAi library. EMBO J. 2002; 21:4429–4438. [PubMed: 12198145]

30. Alsford S, Kawahara T, Glover L, Horn D. Tagging a *T. brucei RRNA* locus improves stable transfection efficiency and circumvents inducible expression position effects. Mol Biochem Parasitol. 2005; 144:142–148. [PubMed: 16182389]

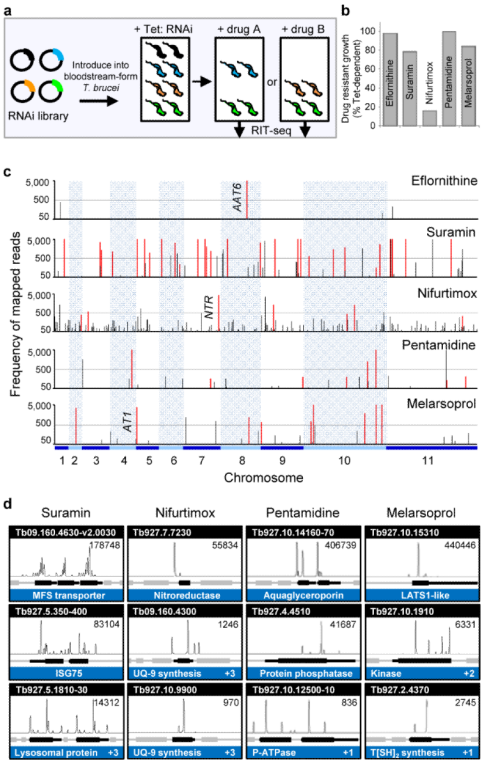

Figure 1. Identification of drug efficacy determinants in *T. brucei*

a, The schematic illustrates the RNAi library screening approach. Expected outcomes are illustrated for RNAi targets that fail to affect drug resistance (black), increase resistance to drug A (blue), drug B (orange) or both (green). **b,** Each screen yielded a population displaying Tet-inducible (RNAi-dependent) drug-resistance; see Supplementary Fig. 1. The plot indicates the proportion of the resistance phenotype that is Tet-inducible. **c,** Genome-wide RIT-seq profiles. Each map represents a non-redundant set of 7,435 protein-coding sequences. Red bars represent 'primary' read-density signatures. Black bars represent all other signatures of >50 reads (see Supplementary data File 1). All three expected 'hits', *AAT6*, *AT1* and *NTR*, are indicated. **d,** Selected signatures. Each peak represents a unique RIT-seq tag. '+', numbers of additional genes identified in each category. See Supplementary Figure 2 for details and additional signatures.

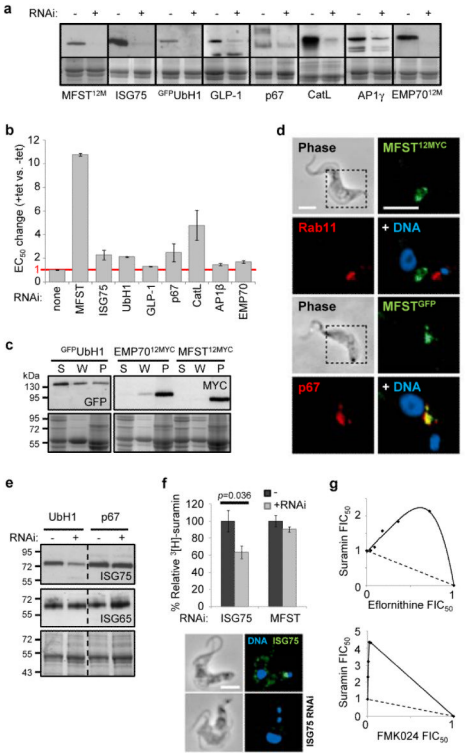

Figure 2. A network of proteins link ISG75, endocytosis and lysosomal functions to suramin action

a, Western blots demonstrate knockdown; Coomassie stains serve as loading controls. See Supplementary Fig. 3 for growth curves. **b,** Endosomal/lysosomal factors and ISG75 contribute to suramin action. Error bars, s.d. from independent RNAi strains; see Supplementary Fig. 4. **c,** MFST and EMP70 are membrane-associated. The western blots show supernatant (S), wash (W) and pellet (P; membrane-fraction). **d,** MFST co-localises with lysosomal protein, p67, but not recycling endosomes (Rab11). **e,** Knockdown of UbH1 specifically decreases ISG75 expression. **f,** ISG75 mediates suramin binding. Error bars, s.d. from duplicate experiments. *P* value from Student's *t*-test. ISG75 knockdown is shown. Scale bar, 5 μm. **g,** CatL/CatB and ODC inhibitors, FMK024 and eflornithine, respectively, antagonise suramin action. Isobolograms showing 50% fractional inhibitory concentrations (FICs). The solid lines indicate antagonism. The dashed lines indicate expected outcomes for no interaction.

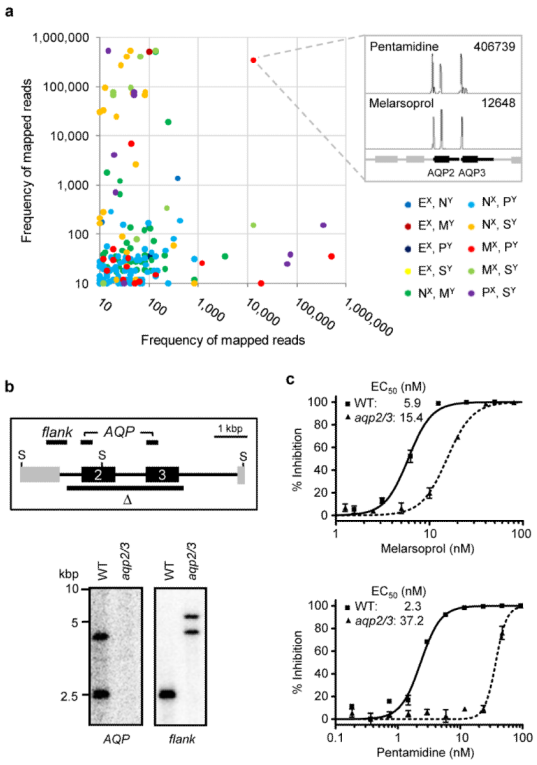

Figure 3. *aqp2/3* null cells are melarsoprol, pentamidine cross-resistant

a, Analysis of read-density for all (74,350) possible pair-wise comparisons of a non-redundant *T. brucei* gene set; E, eflornithine; M, melarsoprol; N, nifurtimox; P, pentamidine; S, suramin; ^{X} and ^{Y}, axes representing each dataset. The box on the right shows the read-density signatures for this locus (Tb927.10.14160-70). **b,** *AQP2/3* knockout was confirmed by Southern blotting. S, *Sac*II; Δ, the region deleted; bars indicate probes. **c,** EC_{50} analysis indicates melarsoprol, pentamidine cross-resistance in *aqp2/3* null cells. Error bars, s.d. from triplicate assays and independent null strains.

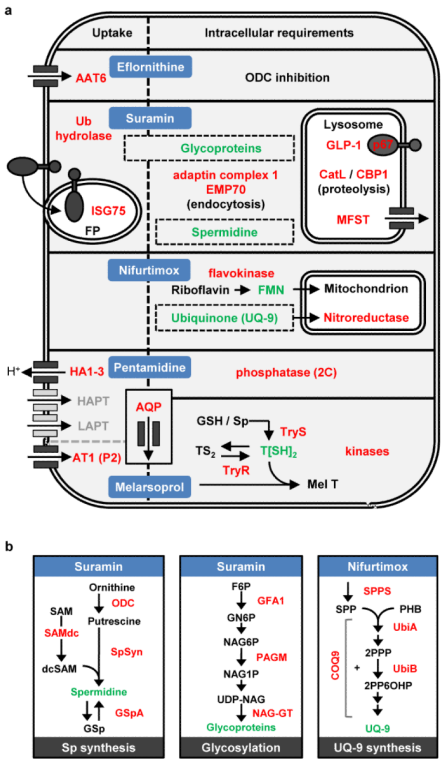

Figure 4. Determinants of drug efficacy in African trypanosomes

Proteins and metabolites linked to drug action are identified by red and green text, respectively. **a,** The schematic summarises the findings from the RIT-seq screens. In the case of suramin, we propose that ISG75 binds the drug at the cell surface. ISG75 trafficking then delivers the complex, via the flagellar pocket (FP), to the endosomal system, leading to accumulation in the lysosome where the drug is liberated by proteases. The MFST may deliver the drug to the cytosol. HAPT/LAPT, high/low-affinity pentamidine transporters; TS_2, oxidised trypanothione; $T[SH]_2$, reduced trypanothione. **b,** Biosynthetic pathways linked to drug action. See text and Supplementary data File 1 for acronyms and further details.